Malaysian Journal of Analytical Sciences (MJAS)





SYNTHESIS OF TIN DOPED ZINC OXIDE (TZO) NANOWIRES: EFFECT ON DYE ADSORPTION

(Synthesis Zink Oksida Nanodawai Terdop Timah: Kesan Kepada Penjerapan Pewarna)

Nur Fairuz Rostan^{1,2}, Mohd Firdaus Malek^{1,2,*}, Maryam Mohammad^{1,2,3}, Nurul Zulaikha Mohd Zambri^{1,2}, Nurfatini Atiqrah Khairul Azhar^{1,2}, Zahidah Othman^{1,2}, Kevin Alvin Eswar^{1,2,4}, Irmaizatussyehdany Buniyamin^{1,2}, Noor Asnida Asli^{1,2}, Mohd Yusri Abdul Rahman⁵, Mohamad Hafiz Mamat⁶ and Mohamad Rusop Mahmood^{1,6}

¹NANO-SciTech Lab, Centre for Functional Materials and Nanotechnology,
Institute of Science, Universiti Teknologi MARA, 40450 Shah Alam, Selangor, Malaysia

²Faculty of Applied Sciences,
Universiti Teknologi MARA, 40450 Shah Alam, Selangor, Malaysia

³Department of Physics, Faculty of Applied Sciences,
Universiti Teknologi MARA, Perak Branch, Tapah Campus, Tapah Road, 35400 Perak, Malaysia

⁴Faculty of Applied Sciences,
Universiti Teknologi MARA, Sabah Branch Tawau Campus, 91032 Tawau, Malaysia

⁵Institute of Microengineering and Nanoelectronics,
Universiti Kebangsaan Malaysia, 43600, Bangi, Selangor, Malaysia

⁶NANO-ElecTronic Centre, School of Electrical Engineering, College of Engineering,
Universiti Teknologi MARA, 40450 Shah Alam, Selangor, Malaysia

*Corresponding author: mfmalek07@uitm.edu.my

Received: 19 September 2023; Accepted: 21 April 2024; Published: 29 June 2024

Abstract

In this study, pristine zinc oxide (ZnO) and tin doped zinc oxide (TZO) nanowires (NWs) had been synthesised on a fluorine doped tin oxide glass substrate via a microwave-assisted ultrasonic irradiation technique. This is a facile and rapid technique that combined ultrasonic irradiation technique during preparation of precursor solution with microwave assisted hydrothermal technique during synthesisation of nanowires. The ultrasonic irradiation technique helps to breakdown the agglomerated and large molecules inside the precursor solution mixture into smaller molecules. The microwave assisted technique helps to increase the temperature of the precursor solution from internal to external in shorter time through the increasing of interaction between molecules. It is important to produce a wide surface area of this material in the photoanode of dye-sensitive solar cells (DSSCs) configuration. Specifically, dye adsorption was an important aspect to grasp, as it can be reflected in the performance of the DSSC device. The concentrations of tin, Sn dopant were varied between 0.3 and 1.8 at.%. As-prepared ZnO and TZO NWs were analysed using field emission scanning electron microscopy and X-ray diffraction. Then, the samples that were soaked in N719 were analysed with ultraviolet-visible-near infrared spectroscopy. The (002) peak of pristine ZnO was regressed, and the identified (100) and (101) peaks of ZnO were slightly shifted towards higher degrees after the addition of Sn dopants. The surface morphology of TZO NWs had displayed a more uniform transformation, with the smallest crystallite size at 51 ± 11 nm (0.9 at.%) due to the enhanced surface area. Unfortunately, it continued to degenerate for concentrations ranging from 1.2 to 1.8 at.%. Urbach energy analysis also suggested that the lowest defect at 0.9 at.% TZO (76 meV) produced the highest crystallinity with a less disorderly thin film. These properties had upheld the dye adsorption and trapping in the ZnO-based thin film. Thus, TZO NWs were the most promising candidates as photoanodes in DSSCs.

Keywords: crystallinity, dye adsorption, microwave, zinc oxide, tin doped

Abstrak

Dalam kajian ini, zink oksida tulen dan zink oksida terdop timah nanodawai telah disintesis ke atas substrat kaca timah oksida terdop florin menggunakan teknik penyiaran ultrasonik bantuan mikrogelombang. Teknik mudah dan pantas ini merupakan hasil gabungan teknik penyiaran ultrasonik yang digunakan semasa proses penyediaan larutan prekursor dengan teknik hidroterma bantuan mikrogelombang yang digunakan semasa proses pensintesisan nanodawai. Teknik penyiaran ultrasonik dapat membantu penguraian molekul yang beraglomerat dan besar dalam campuran larutan prekursor menjadi molekul yang lebih kecil. Teknik bantuan mikrogelombang pula dapat meningkatkan suhu larutan prekursor dari dalaman ke luaran dalam masa yang singkat melalui peningkatan interaksi antara molekul. Penghasilan kawasan permukaan yang luas merupakan aspek yang amat penting bagi bahan fotoanod dalam konfigurasi sel suria pekaan pewarna. Secara khusus, penjerapan pewarna merupakan aspek penting kerana ia akan mencerminkan prestasi peranti sel suria pekaan pewarna. Kepekatan dopan timah telah divariasi dalam lingkungan 0.3 hingga 1.8 peratusan atom. Zink oksida tulen dan zink oksida terdop timah nanodawai yang tersedia telah dianalisis menggunakan mikroskopi elektron pengimbasan pancaran medan dan pembelauan sinar-X. Kemudian, sampel yang telah direndam dalam pewarna N719 dianalisis dengan spektroskopi ultralembayung-cahaya nampak-inframerah dekat. Puncak utama (002) pada zink oksida tulen telah susut dan puncak-puncak identiti melibatkan puncak (100), (002) dan (101) milik zink oksida telah beranjak ke arah yang tinggi setelah penambahan dopan timah. Morfologi permukaan zink oksida terdop timah nanodawai memperlihatkan perubahan ke arah keseragaman dengan saiz kristal paling kecil pada 51 ± 11 nm (0.9 peratusan atom) disebabkan kawasan permukaan dipertingkat, namun terus merosot pada julat kepekatan 1.2 – 1.8 peratusan atom. Analisis tenaga Urbach juga mencadangkan terdapat kecacatan terendah pada 0.9 peratusan atom zink oksida terdop timah (76 meV) dengan menghasilkan saput tipis yang berhabluran tertinggi dan kurang ketaktertiban. Sifat-sifat tersebut telah menyumbang kepada penjerapan pewarna dan pemerangkapan dalam saput nipis berasaskan zink oksida. Oleh itu, zink oksida terdop timah nanodawai adalah calon berpotensi menjadi fotoanod dalam sel suria pekaan pewarna.

Kata kunci: habluran, penjerapan pewarna, gelombang mikro, zink oksida, terdop timah

Introduction

Dye-sensitized solar cell (DSSC) is an emerging thirdgeneration technology in the photovoltaic field. This alternative may provide cleaner and replenishable energy sources for future generations by reducing carbon footprints. The basic structure of DSSC consists of a substrate with a conductive layer, a photoanode, a dye, an electrolyte, and a cathode. Photoaode and cathode are also known as working electrodes and counter electrodes, respectively. According to Green et al.'s 61st version of the solar cell efficiency table, Ecole Polytechnique Fédérale de Lausanne (EPFL) recorded the most recent DSSC efficiency at 12.25% [1]. Compared to other types of third-generation emerging solar cells, DSSCs' efficiencies progressed in small steps. We identified the photoanode layer as one of the major factors that limited the efficiency of DSSCs. The most commonly used photoanode was titanium dioxide (TiO₂). The irregular electric channels in TiO₂ trigger issues, leading to recombination that significantly impacts solar cell performance [2, 3].

The other alternative to TiO₂ was an II-VI semiconductor combination of zinc and oxide from metal and chalcogen elements that can create vast application materials. Zinc oxide (ZnO) is a benign, abundantly available, and thermally stable material. Zinc oxide nanostructure can be found in zero

dimensions as nanodots [4] or nanoparticles [5], one dimensions as nanowires (NWs) [6] or nanorods [7], two dimensions as nanosheets [8] or nanoplates [9] and three dimensions as nanoflakes [10] or nanoflowers [11]. Based on previous studies, there are a few approaches to grow one-dimension (1D) ZnO nanostructures that include chemical bath deposition [12], hydrothermal [13], wet chemistry [14], solvothermal [15] and water bath [16]. However, these methods require longer reaction times, complex processes, and high-end instruments. For instance, the study conducted by Dloo et al. have found that using the hydrothermal technique required more than 2 hours to synthesis ZnO NWs [17]. Syrrokostas and his team have utilised chemical bath deposition process for 7 hours to form ZnO NWs that achieved the desired morphology [18]. Other than that, Guo et al. has managed to grow ZnO NWs within 1.5 hours using microwave assisted hydrothermal process [19]. However, the synthesisation process was utilising modified commercial oven that could inject the precursor solution continuously during the reaction. Thus, a rapid and straight-forward technique would be beneficial to the current technology of ZnO NWs synthesis.

The porosity of the photoanode compound directly influences dye adsorption, conductivity, and charge

transport across the DSSC [20]. A branched ZnO photoanode has the advantage of increasing dye adsorption properties by filling the space between the NW structures [21]. Previous studies have found that tin, Sn has a compatible structure as it has a lower ionic radius (Sn⁴⁺ ion: 0.69 Å) compared to Zn²⁺ ion with an ionic radius of 0.74 Å [22]. Therefore, at low doping concentrations, the oxide lattice remains unaffected [23]. Besides, Sn helps to improve the surface properties by increasing the surface area of ZnO thin film via the formation of smaller crystallite sizes than pure ZnO [24]. The doping of Sn must be controlled (below 2 at.%) to prevent clumping undesired truncated coneshaped nanostructure that can affect the quality of ZnO thin film [25]. Sn also has the ability to improve electrical conductivity in a ZnO photoanode by enhancing the carrier concentration by introducing double-charge carriers [26]. This situation is favourable to boost the efficiency of DSSC [22, 23]. This study had combined the environmental-friendly ultrasonic irradiation with rapid microwave assisted technique to synthesis pristine ZnO and tin doped ZnO (TZO) NWs. These 1D TZO NWs were synthesised by varying the dopant concentrations (atomic percentage, at.%) to identify the optimum properties for DSSC photoanode applications.

Materials and Methods

The procedures are categorised based on step-by-step processes involved to synthesis and analyse the properties of pristine ZnO and TZO thin film that grown on FTO glass substrate.

TZO NWs thin film growth

The FTO glass was specified into 0.11 cm thickness and 2 \times 2 cm² sized substrates. Then, aluminium doped ZnO seed layer had deposited on oxide-free substrate using spin coating technique [27]. Followed by that, tin doped ZnO (TZO) NWs were grown via microwave-assisted ultrasonic irradiation method was carried out. An equimolar of 12.5 mM of zinc acetate dihydrate, Zn(CH₃COO)₂·2H₂O; hexamethylenetetramine, C₆H₁₂N₄ (HMTA) and tin (IV) chloride pentahydrate, SnCl₄·5H₂O powder were used as precursor, stabiliser and dopant, respectively. The amount of Sn dopant was varied to 0.3 – 1.8 at.%. All the reagents were dissolved

in a beaker filled with 1000 mL distilled water that acted as solvent or medium for the reaction. Then, the mixture solution was stirred at 80 °C for 40 minutes to yield clear and homogeneous solution. Next, the mixture solution was sonicated at 50 °C for 30 minutes using an ultrasonic water bath (Hwasin Technology Powersonic 405, 40kHz) and aged for 60 minutes at room temperature. After that, the mixture solution is continued to age at room temperature with stirring at speed of 3. The solution was poured into a Schott bottle. Then, the optimized seed layer-coated glass substrates were placed at the bottom of the Schott bottle with one substrate each. Afterward, the container was placed inside the microwave oven (SHARP 25 L Microwave Oven with Grill R754AST) which was set to power of 600 W and microwaved for 60 minutes. The excess nanostructures deposited on the substrates were rinsed with distilled water thoroughly. After that, the samples were annealed (hard-baked) in a preheated furnace at 500 °C for 60 minutes. Finally, the samples were removed from furnace for fast cooling process and proceeded with further analyses. The as-prepared pristine ZnO and TZO NWs grown on FTO were characterised with X-ray diffraction (XRD) to investigate the crystal orientations and crystallinity of the samples. The XRD model used was PANalytical X'Pert PRO with Cu K-alpha radiation wavelength of 1.5419 Å. The crystallite size was calculated based on the Scherrer formula provided in Equation 1. The k in this equation was the Scherrer constant with the value of 0.94. The λ represented the X-ray wavelength (CuK_{α} = 1.5419 Å), β denoted as the line broadening at full width half maximum while θ was the Bragg's angle. β and θ were both measured in radians.

$$D = \frac{k\lambda}{\beta\cos\theta} \tag{1}$$

Additionally, dislocation line density (DLD) of the thin films represented the length of dislocation lines per unit volume of the crystal which can be determined using Equation 2.

$$\delta = \frac{1}{D^2} \tag{2}$$

Furthermore, the interplanar distance or known as d-spacing can be figured out by substituting θ , n and λ

which were Bragg's angle, order of diffraction and wavelength of X-rays, respectively. The order of diffraction usually was 1 for first order. Value of d-spacing can be obtained through the Bragg's law formula in Equation 3.

$$2d\sin\theta = n\lambda\tag{3}$$

Besides that, Field Emission Scanning Electron Microscope (FESEM) to identify the morphology and particle distributions. The FESEM model utilised was Analytical High Resolution Field Emission Scanning Electron Microscope Apreo 2S (Thermo Fischer Scientific). The surface morphology images of the samples were taken at 10 kV and 60 000x magnification. Further analyses were done using ultraviolet-visiblenear infrared (UV-vis-NIR) spectroscopy to analyse the defects in the samples. The UV-vis-NIR model used was Carry 5000 Varian with the fixed spectral range of 300 – 1200 nm. The data from UV-vis-NIR were analysed to obtain the Urbach energy value. The absorption coefficient was fitted to exponential function of energy. The derived formula of Urbach energy involved in this study was listed in Equation 4 and 5. The most linear gradient of plotted $\ln \alpha$ against photon energy (hv) was enabled the gaining of Urbach energy value.

$$\alpha = \alpha_0 \exp\left(\frac{hv}{E_u}\right) \tag{4}$$

$$\ln \alpha = \left(\frac{1}{E_u}\right) hv + \ln \alpha_0 \tag{5}$$

Dye adsorption and desorption process

Dye loading process was performed on pristine ZnO and TZO NWs thin film in order to analyse the adsorption

and desorption ability of the photoanode. Dye that has been chosen as the light sensitizer in this study was a ruthenium-based dye namely Di-tetrabutylammonium (isothiocyanato) bis (2,2'-bipyridyl-4,4'cis-bis dicarboxylato) ruthenium (II) or also known as N719. 0.5 mM of ethanolic N719 dye solution was allowed to be stirred homogenously at room temperature before ready to be used. FTO glass substrate with each type of NWs photoanode were then soaked into the prepared solution for 24 hours. The soaked sample was picked up and dried from excess dye solution. Then, dye loading process was carried out to analyse the adsorb and desorb action of photoanode thin film. Equation 1 was used to measure the dye loading in photoanode. Dye loading of photoanode thin film was determined by the multiply of dye concentration and volume of solution which then divided by the electrode area. The unit for dye loading in Equation 6 was mol/cm² while M denoted as dye concentration in mol/L, volume, V in unit of L and A was the electrode area in cm². The size of area covered with electrode was controlled at 3.6 cm². The dye loading value was consistent for all pristine ZnO and TZO thin films which was 0.833 µmol/cm². The dye loading value was smaller compared to other studies due to the large dye exposed surface area.

$$Dye \ loading = \frac{M \times V}{A} \tag{6}$$

The FTO glass/ZnO SL/pristine ZnO or TZO NWs/N719 dye configuration was illustrated as in Figure 1. Next step was the samples were washed with ethanol during unloading process to study the desorption of the photoanode. The transmittance of dye adsorbed and desorbed for all samples were plotted and discussed further in Results and Discussion section.

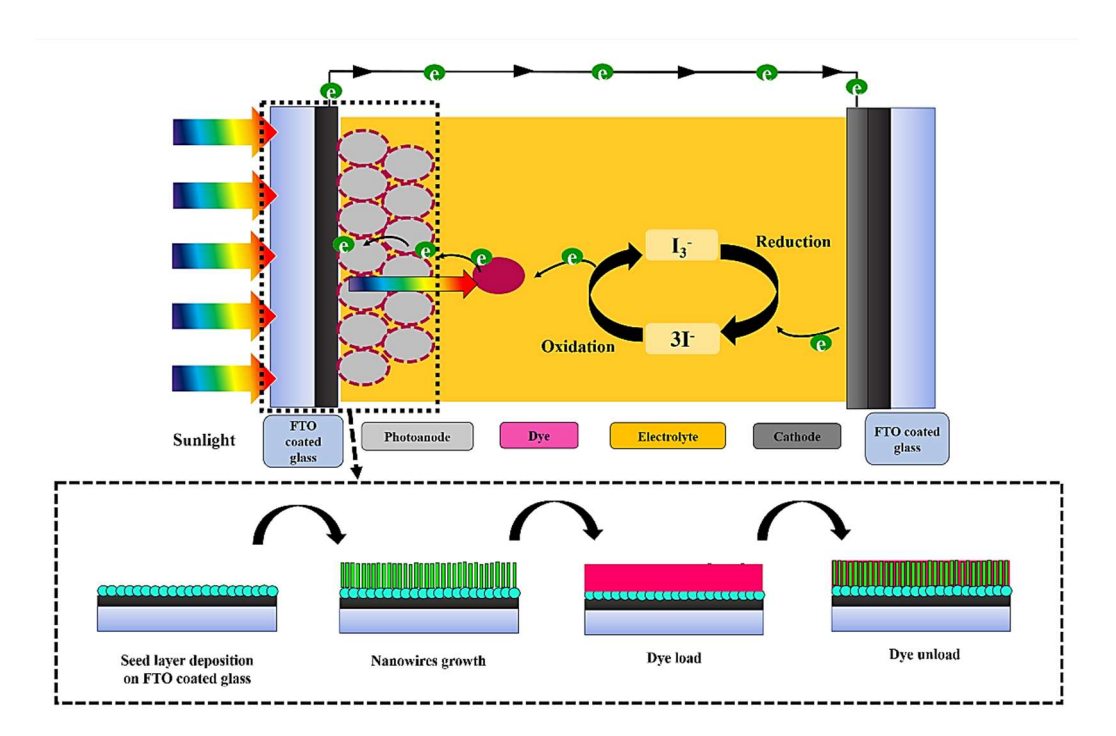


Figure 1. Stepwise processes that involved NWs photoanode formation and dye adsorb-desorb actions that build up DSSC configurations

Results and Discussion

This section presented the results and some elaboration based on physical and optical properties analysis that had been investigated on ZnO-based thin film. The analyses done were discussed in detailed based on each subtopic.

Crystal orientation and crystallinity analysis

The XRD pattern shown in Figure 2 (a) and Figure 2 (b) had indicated the hexagonal wurtzite structure with existence of peaks (100), (002), (101), (102), (110), (103) and (112) at 2θ of 32.29° , 34.96° , 38.35° , 52.11° , 57.06° , 62.17° and 66.26° . These peaks were the blueprints of pristine ZnO material according to JCPDS 00-036-1451. The small peak at 34.5° was belonged to FTO [28]. After the addition of Sn as dopants (0.3 – 1.8 at.%), the same peaks remained without any appearance of additional peak. After doped, the major peaks within the range of 30-40 degrees had slightly shifted to higher degree positions. Previous work on studying the

effect of dopant concentration also had identified comparable tendency such as in this work [11]. This increment had suggested that there was shrinkage in dspacing due to the consequence of compressive stress [29]. The slightly difference in atomic radii of Zn²⁺ ion with Sn⁴⁺ ion at 0.69 Å had shifted the 2θ crystal positions to relatively higher value [22]. The most dominant (002) peak that observable in pristine ZnO sample was suppressed and left with (101) as the most significant major peak after Sn dopant was added. This trend also can be noticed from earlier study by varying the Sn dopants in 2 - 8 wt.% [22]. The crystallite size and interplanar distance of pristine and all TZO samples had shown similar trends which indicated that both factors were closely related to each other. On the other hand, the FWHM and dislocation line density had the opposite relationship with the other two factors which mentioned before. These patterns can be seen from previous studies done by other researchers [29, 30].

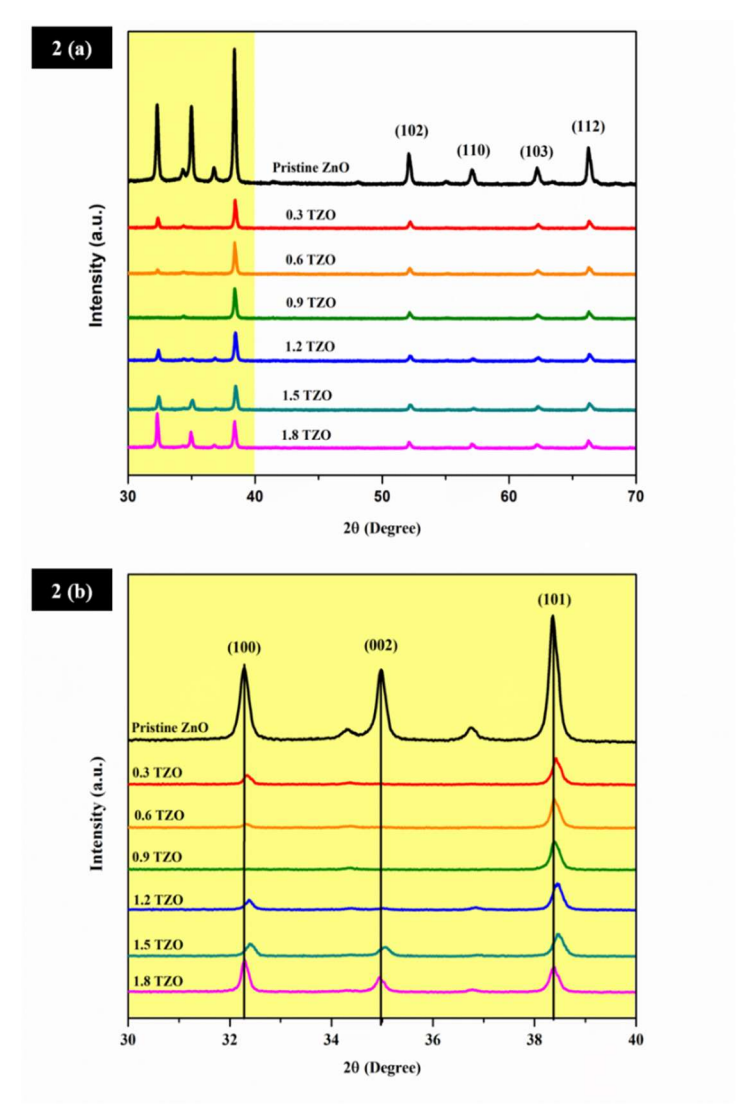


Figure 2. XRD patterns of pristine ZnO and various TZO samples within the range of (a) 30 - 70 degrees and (b) 30 - 40 degrees

Table 1. Crystallite size, dislocation line density and interplanar distance of pristine and varied TZO samples at (101) plane

(-+-) F				
Sample	FWHM	Crystallite Size	Dislocation Line	Interplanar
Sample	(Degree)	(nm)	Density (E14 m ⁻²)	Distance (Å)
Pristine ZnO	0.214	41.09	5.92	2.347
0.3 TZO	0.223	39.44	6.43	2.340
0.6 TZO	0.203	43.32	5.33	2.344
0.9 TZO	0.214	41.09	5.92	2.344
1.2 TZO	0.232	37.91	6.96	2.341
1.5 TZO	0.244	36.05	7.70	2.340
1.8 TZO	0.223	39.43	6.43	2.345

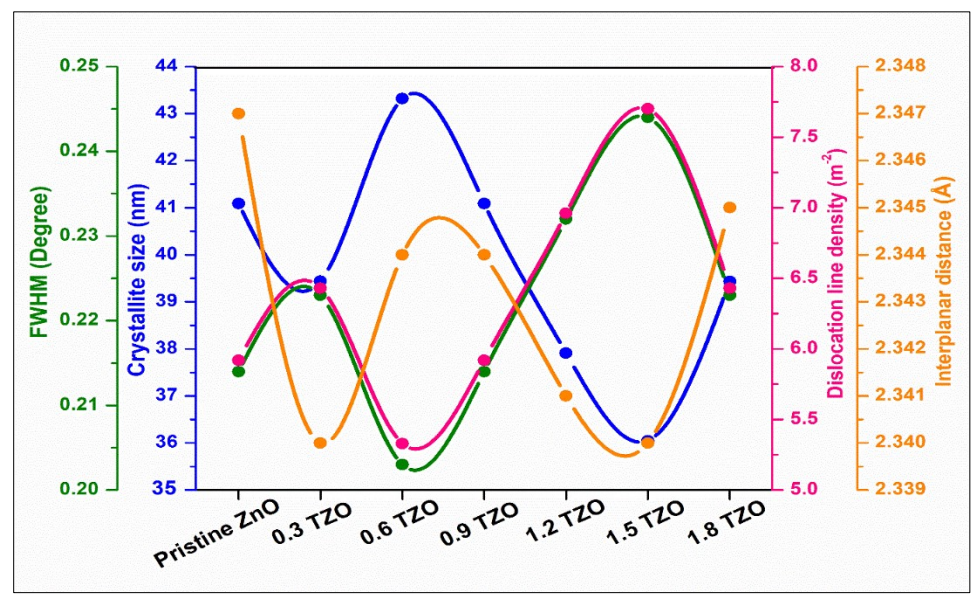


Figure 3. The crystallite size, dislocation line density and interplanar distance of pristine ZnO and varied TZO samples at (101) plane

Surface morphology and uniformity analysis

FESEM images had displayed pristine ZnO and TZO (0.3 - 1.8 at. %) NWs in Figure 4 (a - g). The particle size decreased and uniformity increased with the increment in Sn dopant concentration in ZnO to form nanowires. High in uniformity is one of the crucial aspects to produce decent morphological, optical and electrical properties. The smallest and most uniform TZO nanowire structures had displayed at 0.9 TZO (51 \pm 11 nm). The introduction of Sn ions had changed the lattice of ZnO due to difference in ionic radius between Sn4+ ions (0.69 Å) and Zn^{2+} ions (0.74 Å) [22]. In contrary, after this point (1.2 at.% onwards), the nanowire structures started to show non-uniformity trend and become agglomerated and deformed. This phenomenon occurred due to Ostwald ripening effect which small crystals pick up the excess solute and amalgamate into large nanostructures [31]. This defect can be observed via FESEM surface images after excess Sn was doped (1.5 and 1.8 TZO). Previous researchers had suggested that the doping of tin must be restrained under 2 at.% to prevent clumping undesired truncatedcone shaped nanostructure which may disturb the quality of ZnO thin film [25]. Thus, this agglomerated nanostructures are expected to affect the resistivity and worsen the electrical properties of the photoanode thin film [25]. The summarised data on average particle size for all samples were tabulated in Table 2.

Defect analysis

Urbach energy indicates the degree of structural disorder, defects, and impurities in the material. High in Urbach energy translate into high defects density, more disorder and low in crystallinity. The defects can generate localised states that can traps carriers (electron and hole) and caused recombination. 0.9 TZO in Figure 5 had shown the lowest Urbach energy (76 meV) which reflected through the most uniform average particle size obtained in FESEM analysis and had achieved near lowest FWHM (0.214°) and dislocation line density (5.92 E14 m⁻²). The Urbach energy values for all samples were tabulated in Table 3.

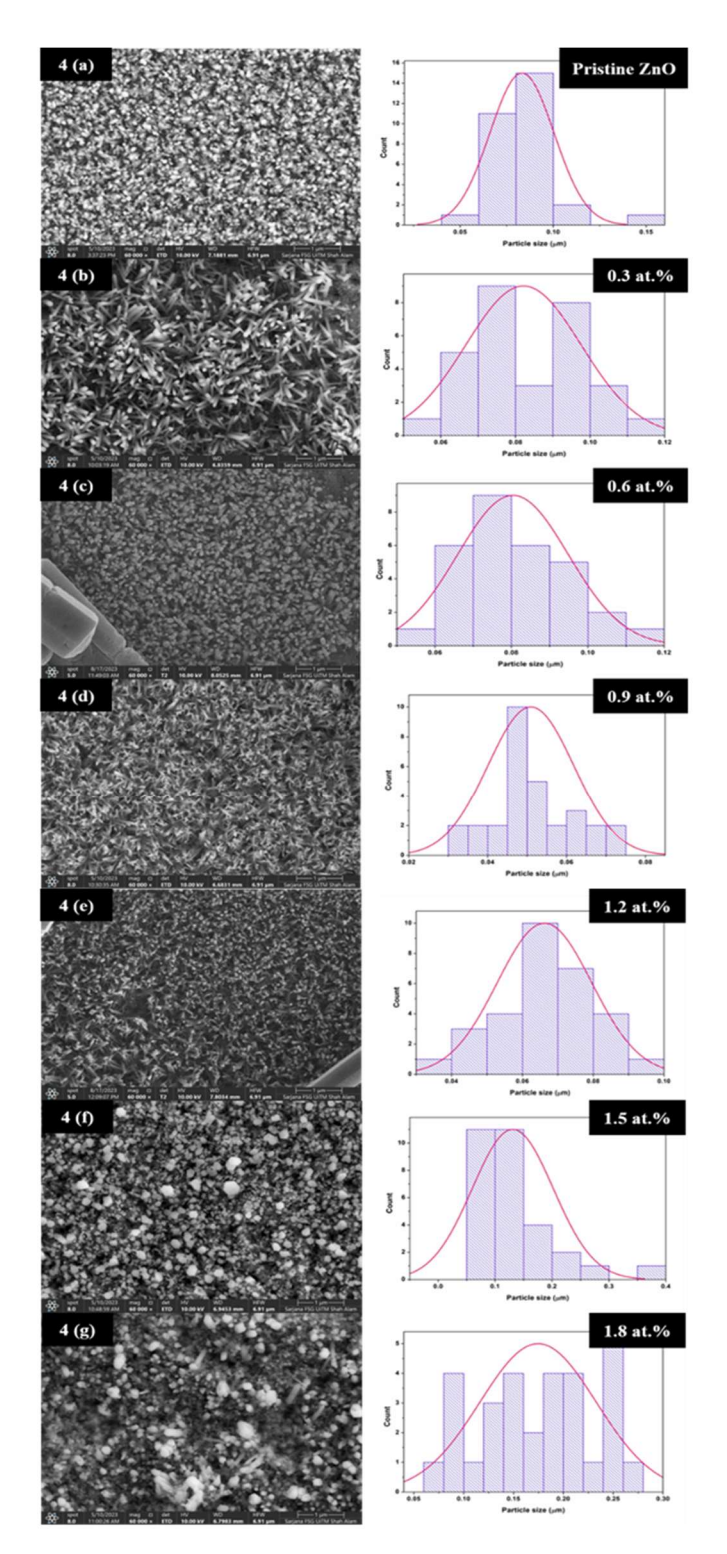


Figure 4. FESEM images and particle distributions of (a) pristine ZnO and $(b-g)\ 0.3-1.8$ at.% of TZO NWs

Table 2. The average particle size from particles distribution analysis in FESEM images for each sample

Label in Figure 4	Sample	Average Particle Size (nm)	
(a)	Pristine ZnO	83 ± 17	
(b)	0.3 TZO	82 ± 15	
(c)	0.6 TZO	80 ± 14	
(d)	0.9 TZO	51 ± 11	
(e)	1.2 TZO	66 ± 13	
(f)	1.5 TZO	131 ± 71	
(g)	1.8 TZO	175 ± 58	

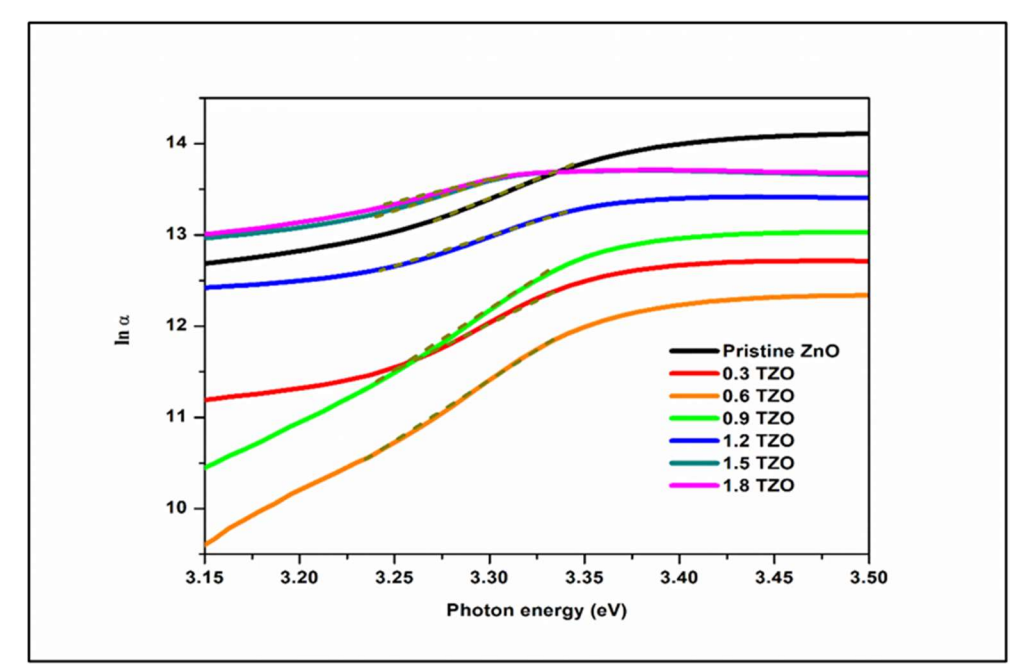


Figure 5. Plot of ln α against photon energy of pristine ZnO and 0.3 – 1.8 at.% of TZO NWs

Table 3. Urbach energy of pristine ZnO and 0.3 - 1.8 at.% of TZO NWs

Sample	Urbach Energy (meV)
Pristine ZnO	111
0.3 TZO	98
0.6 TZO	77
0.9 TZO	76
1.2 TZO	161
1.5 TZO	175
1.8 TZO	176

Dye adsorption and desorption analysis

From the plotted UV-vis-NIR graphs in Figure 6 (a - g)and the summarised data in Table 4 had found that the transmittance patterns of pristine ZnO was boosted with the helped of Sn dopants. This was due to the fact that Sn had successfully reduced the particle size as shown in FESEM images. However, the pattern had started to deteriorate after 1.2 TZO samples as the transmittance started to drop in respond to inhomogeneity of the NWs formation. For the dye adsorption ability, the transmittance of the window layer is reduced at the specific wavelengths corresponding to the dye's absorption peaks. The transmittance recorded by N719 dye was 13.50%. Numerous previous studies had discovered that this type of dye was one of the most promising and highly potential candidates for DSSC sensitiser application [32, 33]. The increased in the incident light absorbed by the dye molecules which resulted in a higher probability of generating electronhole pairs. In this case, adsorbed dye molecules on ZnO nanostructures had maintained its adsorption even after desorption process (based on Table 4) was favourable for DSSC photoanode application. This strong bonding between dye molecules and metal oxide nanostructures were helpful for charge injection movement, dye functioning and generating the stability of solar cell performance [34]. There was not much difference in transmittance level during adsorption and desorption actions for pristine ZnO (1.25%), 0.3 TZO (2.71%), 1.2 TZO (2.21%), 1.5 TZO (5.28%) and 1.8 TZO (0.91%). This situation had established the dependability of better dye trapping character on the multiplane crystal orientation. The same pattern also displayed through less efficient dye trapping effect on 0.6 (7.79%) and 0.9 TZO (9.95%) due to much larger difference in trasnmittance before and after desorption process. This might due to the crystal growth leaned towards single plane (101). Less efficient dye trapping properties can be improved via application of buffer layer on top of the structure.

Table 4. The average transmittance within visible region (400 – 800 nm) of pristine ZnO and various TZO samples

Label in Figure 4	Sample	Average Transmittance (%)		
		As-prepared Sample	Dye Adsorbed (S1)	Dye Desorbed (S2)
(a)	Pristine ZnO	71.49	18.13	19.38
(b)	0.3 TZO	73.31	15.64	18.35
(c)	0.6 TZO	78.68	46.32	54.11
(d)	0.9 TZO	78.03	40.80	50.75
(e)	1.2 TZO	56.48	33.12	35.33
(f)	1.5 TZO	50.22	44.99	50.27
(g)	1.8 TZO	47.56	41.08	41.99

Conclusion

TZO nanowires with the desired properties were successfully synthesized using facile and ultrarapid microwave assisted ultrasonic irradiation technique. High uniformity, more crystalline, low defect, high transmittance and acceptable dye adsorption properties are the qualities can be found in 0.9 TZO thin film. Crystallinity can greatly influence the electrochemical stability of the thin film. The recombination will be suppressed if the defect level is low. Thus, this optimised TZO photoanode is expected to boost the efficiency and performance of DSSCs. Therefore, the fabrication of DSSCs is one of the ways to pave the pathway towards refining the future of renewable and

clean energy generation.

Acknowledgement

All authors would like to highlight the appreciation towards Universiti Teknologi MARA (UiTM) for funding this project under Research Grant No. 600-RMC/GIP5/3 (020/2023) and 600-RMC/GPMCOE5/3 (106/2022). Besides that, we also would like to acknowledge the contributions by Faculty of Applied Sciences and NANO SciTech lab, Centre for Functional Materials & Nanotechnology, Institute of Science under UiTM.

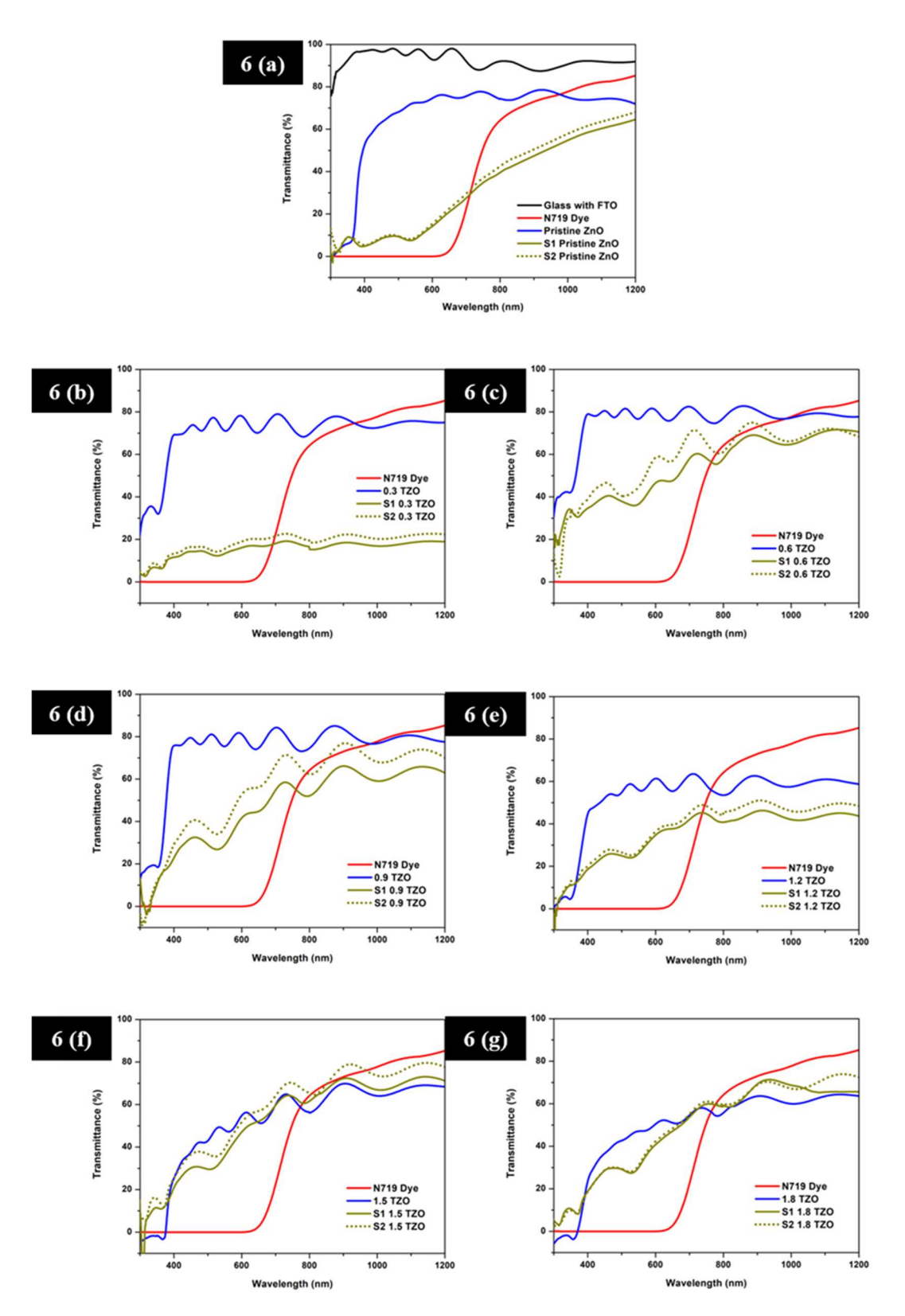


Figure 6. Transmittance of (a) pristine ZnO and (b - g) 0.3 - 1.8 at.% TZO NWs with dye adsorbed and desorbed plot

References

- Green, M. A., Dunlop, E. D., Siefer, G., Yoshita, M., Kopidakis, N., Bothe, K., and Hao, X. (2023). Solar cell efficiency tables (Version 61). *Progress in Photovoltaics: Research and Applications*, 31(1): 3-16.
- 2. Mohammadian-Sarcheshmeh, H., Arazi, R., and Mazloum-Ardakani, M. (2020). Application of bifunctional photoanode materials in DSSCs: A review. *Renewable and Sustainable Energy Reviews*, 134: 110249.
- Bhatti, K. A., Khan, M. I., Saleem, M., Alvi, F., Raza, R., and Rehman, S. (2019). Analysis of multilayer based TiO₂ and ZnO photoanodes for dye-sensitized solar cells. *Materials Research Express*, 6(7): 075902.
- 4. Ramya, M., Nideep, T. K., Nampoori, V. P. N., and Kailasnath, M. (2021). Solvent assisted evolution and growth mechanism of zero to three dimensional ZnO nanostructures for dye sensitized solar cell applications. *Scientific Reports*, 11(1): 9.
- Chen, H.-Y., Huang, B.-Y., Koo, H.-S., and Huang, M.-T. (2020). Characterization of dye-sensitized solar cells based on various CaCO₃-doped ZnO photoanodes prepared using wet powder mixing and grinding. *Optik*, 220: 164899.
- 6. Nikoobakht, B., Wang, X., Herzing, A., and Shi, J. (2013). Scalable synthesis and device integration of self-registered one-dimensional zinc oxide nanostructures and related materials. *Chemical Society Reviews*, 42(1): 342-365.
- Fonseca, A. F. V. D., Siqueira, R. L., Landers, R., Ferrari, J. L., Marana, N. L., Sambrano, J. R., La Porta, F. D. A., and Schiavon, M. A. (2018). A theoretical and experimental investigation of Eudoped ZnO nanorods and its application on dye sensitized solar cells. *Journal of Alloys and Compounds*, 739: 939-947.
- 8. Lin, C.-Y., Lai, Y.-H., Chen, H.-W., Chen, J.-G., Kung, C.-W., Vittal, R., and Ho, K.-C. (2011). Highly efficient dye-sensitized solar cell with a ZnO nanosheet-based photoanode. *Energy & Environmental Science*, 4(9): 3448-3455.
- 9. Kołodziejczak-Radzimska, A., and Jesionowski, T. (2014). Zinc oxide—from synthesis to application: A review. *Materials*, 7(4): 2833-2881.
- 10. Das, A., Wary, R. R., and Nair, R. G. (2020). Cu modified ZnO nanoflakes: An efficient visible light-driven photocatalyst and a promising photoanode for dye sensitized solar cell (DSSC). *Solid State Sciences*, 104: 106290.
- 11. Zhuang, S., Lu, M., Zhou, N., Zhou, L., Lin, D., Peng, Z., and Wu, Q. (2019). Cu modified ZnO

- nanoflowers as photoanode material for highly efficient dye sensitized solar cells. *Electrochimica Acta*, 294: 28-37.
- Tayyaba, S., Ashraf, M. W., Tariq, M. I., Akhlaq, M., Balas, V. E., Wang, N., and Balas, M. M. (2020). Simulation, analysis, and characterization of calcium-doped ZnO nanostructures for dyesensitized solar cells. *Energies*, 13(18): 4863.
- 13. Saboor, A., Shah, S. M., and Hussain, H. (2019). Band gap tuning and applications of ZnO nanorods in hybrid solar cell: Ag-doped verses Nd-doped ZnO nanorods. *Materials Science in Semiconductor Processing*, 93: 215-225.
- Giannouli, M., Govatsi, K., Syrrokostas, G., Yannopoulos, S., and Leftheriotis, G. (2018).
 Factors Affecting the Power Conversion Efficiency in ZnO DSSCs: Nanowire vs. Nanoparticles. *Materials*, 11(3): 411.
- 15. Angaiah, S., Arunachalam, S., Murugadoss, V., and Vijayakumar, G. (2019). A Facile polyvinylpyrrolidone assisted solvothermal synthesis of zinc oxide nanowires and nanoparticles and their influence on the photovoltaic performance of dye sensitized solar cell. ES Energy & Environment, 4: 59-65.
- Saleem, M., Farooq, W. A., Khan, M. I., Akhtar, M. N., Rehman, S. U., Ahmad, N., Khalid, M., Atif, M., Almutairi, M. A., and Irfan, M. (2019). Effect of ZnO Nanoparticles coating layers on top of ZnO nanowires for morphological, optical, and photovoltaic properties of dye-sensitized solar cells. *Micromachines*, 10(12): 819.
- 17. Dloo, A., Fazouan, N., and Atmani, E. H. (2023). Investigation of hydrothermal growth time and temperature for optimized ZnO nanowire arrays toward photovoltaics. *Surfaces and Interfaces*, 40: 103123.
- 18. Syrrokostas, G., Govatsi, K., and Yannopoulos, S. N. (2016). High-quality, reproducible ZnO nanowire arrays obtained by a multiparameter optimization of chemical bath deposition growth. *Crystal Growth & Design*, 16(4): 2140-2150.
- 19. Guo, H., Ding, R., Li, N., Hong, K., Liu, L., and Zhang, H. (2018). Defects controllable ZnO nanowire arrays by a hydrothermal growth method for dye-sensitized solar cells. *Physica E: Low-dimensional Systems and Nanostructures*, 2018: 105.
- Zatirostami, A. (2021). Fabrication of dyesensitized solar cells based on the composite TiO₂ nanoparticles/ZnO nanorods: Investigating the role of photoanode porosity. *Materials Today Communications*, 26: 102033.

- Choudhury, B. D., Lin, C., Shawon, S. M. A. Z., Soliz-Martinez, J., Huq, H., and Uddin, M. J. (2021). A photoanode with hierarchical nanoforest TiO₂ structure and silver plasmonic nanoparticles for flexible dye sensitized solar cell. *Scientific Reports*, 11(1)
- 22. Thirumoorthi, M., and Thomas Joseph Prakash, J. (2019). Doping effects on physical properties of (101) oriented tin zinc oxide thin films prepared by nebulizer spray pyrolysis method. *Materials Science and Engineering: B*, 248: 114402.
- Nunes, V. F., Lima, F. M., Teixeira, E. S., Júnior, P. H. F. M., Almeida, A. F. L., and Freire, F. N. A. (2021). Effects of tin on the performance of ZnO photoanode for DSSC. *Matéria (Rio de Janeiro)*, 26(4): 1312.
- Khadtare, S., Pathan, H. M., Han, S.-H., and Park, J. (2021). Facile synthesis of binder free ZnO and its Indium, Tin doped materials for efficient dye sensitized solar cells. *Journal of Alloys and Compounds*, 872: 159722.
- 25. Xu, L., Zheng, G., Xian, F., and Su, J. (2019). The morphological evolution of ZnO thin films by Sn ions doping and its influence on the surface energy and photocatalytic activity. *Materials Chemistry and Physics*, 229: 215-225.
- Saurdi, I., Mamat, M., Malek, M., and Rusop, M. (2014). Preparation of aligned ZnO nanorod arrays on Sn-doped ZnO thin films by sonicated sol-gel immersion fabricated for dye-sensitized solar cell. Advances in Materials Science and Engineering, 2014: 636725.
- 27. Mamat, M. H., Sahdan, M. Z., Khusaimi, Z., Ahmed, A. Z., Abdullah, S., and Rusop, M. (2010). Influence of doping concentrations on the aluminum doped zinc oxide thin films properties for ultraviolet photoconductive sensor applications. *Optical Materials*, 32(6): 696-699.

- 28. Magiswaran, K., Norizan, M. N., Mahmed, N., Mohamad, I. S., Idris, S. N., Sabri, M. F., Amin, N., Sandu, A. V., Vizureanu, P., Nabiałek, M., and Salleh, M. A. (2023). Controlling the layer thickness of zinc oxide photoanode and the dyesoaking time for an optimal-efficiency dyesensitized solar cell. *Coatings*, 13(1): 20.
- 29. Khan, M. I., Naeem, M., Mustafa, G., Abubshait, S., Mahmood, A., Al-Masry, W., Al-Garadi, N., and Ramay, S. (2020). Synthesis and characterization of Co and Ga co-doped ZnO thin films as an electrode for dye sensitized solar cells. *Ceramics International*, 46: 127.
- Bashir, M. B., Rajpar, A. H., Salih, E. Y., and Ahmed, E. M. (2023). Preparation and photovoltaic evaluation of CuO@Zn(Al)O-mixed metal oxides for dye sensitized solar cell. *Nanomaterials*, 13(5): 802.
- 31. Nanev, C. N. (2023). Thermodynamic and molecular-kinetic considerations of the initial growth of newly born crystals; crystal size distribution; dissolution of small crystals during ostwald ripening due to temperature changes. *Progress in Crystal Growth and Characterization of Materials*, 69(2): 100604.
- 32. Shalini, S., Balasundaraprabhu, R., Kumar, T. S., Prabavathy, N., Senthilarasu, S., and Prasanna, S. (2016). Status and outlook of sensitizers/dyes used in dye sensitized solar cells (DSSC): a review. *International Journal of Energy Research*, 40(10): 1303-1320.
- 33. Sekar, N., and Gehlot, V. Y. (2010). Metal complex dyes for dye-sensitized solar cells: Recent developments. *Resonance*, 15(9): 819-831.
- 34. Tomar, N., Agrawal, A., Dhaka, V. S., and Surolia, P. K. (2020). Ruthenium complexes based dye sensitized solar cells: Fundamentals and research trends. *Solar Energy*, 207: 59-76.